Supporting Information

Deep eutectic solvent boosted ruthenium catalysts for acetylene hydrochlorination

Linfeng Li,[a] Bao Wang,[a] Tiantong Zhang,[a] Haiyang Zhang,[b] Wei Li,[a] Jiangjiexing Wu*[c] and Jinli Zhang*[ab]

[a] School of Chemical Engineering and Technology, Tianjin University, Tianjin, 300072, P.R. China

[b] School of Chemistry and Chemical Engineering of Shihezi University, Shihezi, Xinjiang 832000, P.R. China.

[c] School of Marine Science and Technology, Tianjin University, Tianjin, 300072, P.R. China

*Corresponding authors: Dr. Jiangjiexing Wu, E-mail: wujiangjiexing2007@126.com; Prof. Jinli Zhang, E-mail: zhangjinli@tju.edu.cn.

Table of Contents

1. Experiment

1.1. DFT calculations

Density functional theory (DFT) calculations were performed in Gaussian 09 using the B3LYP function, corrected by the DFT-D3 method to optimise the analysis of the weak interactions.[1, 2] The Ru atoms underwent optimization with the SDD pseudopotential basis set, while the remaining atoms were geometrically optimized utilizing the 6-311G(d,p) basis set.[3, 4] Single-point energies were ascertained through the def2-TZVP basis set, and local energy minima were identified through vibrational frequency calculations.[5-7] The structural optimization's convergence criterion was set to the default Gaussian 09 setting. The energy of adsorption (E_{ad}) is expressed by the following equation:

$$E_{ad} = E_{ad-state} - E_{cat} - E_{reactant} \# \ (1)$$

where $E_{ad\text{-}state}$, $E_{reactant}$, and E_{cat} are terms that denote the adsorption energy of the catalyst concerning the feedstock reactant, the feedstock reactant itself, and the catalyst, respectively.

Furthermore, the distribution of electrostatic potentials on the surface was scrutinized using Multiwfn 3.8 and VMD software.[8, 9] The hydrogen bond energy (E_{HB}) by Atoms-in-molecules (AIM) theory using the electron density at the position of the bond critical point (BCP) of the hydrogen bond, calculated in Equation 2.[10]

$$E_{HB} = -223.08 \times \rho_{BCP} + 0.7423 \# \ (2)$$

Here the E_{HB} is in kcal mol^{-1} and the unit of ρ_{BCP} is in a.u.

1.2. Characterisation of the catalysts

Fourier transform infrared spectroscopy (FT-IR) spectrum was measured using a NICOLET iZ10 infrared spectrometer and was used to analyse changes in molecular structure. Nuclear magnetic resonance hydrogen spectroscopy (^{1}H-NMR) was measured using Bruker AVANCE III 400 MHz with deuterium oxide (D_2O) as the deuterium reagent and was used to observe changes in hydrogen at different positions in the sample. Ultraviolet-visible (UV-Vis) spectra at 190-600 nm were measured using an Agilent Cary 300 spectrophotometer to analyse the interactions between the metal precursors and the ligands. The structural parameters of the samples were determined using Quantachrome Autosorb-iQ to analyse the changes in specific surface area and

pore volume of the catalysts. Thermogravimetric analysis was performed using METTLER TOLEDO TGA/DSC-2 to analyse the amount of carbon deposited on the catalyst after the reaction. X-ray photoelectron spectroscopy (XPS) was measured using Thermo K-Alpha^{+} and was used to determine the valence and relative content of Ru species. High-angle annular dark-field-scanning transmission election microscope (HAADF-STEM) images and elemental mapping analyses were performed using JEM-2100F to observe the dispersion of the active components.

1.3. Catalytic performance evolution

The catalytic performance of the catalyst (2 mL) was evaluated under atmospheric pressure in a fixed-bed quartz reactor (Fig. S15, o.d. of 10 mm, i.d. of 8 mm). Before the reaction, the reactor was purged with a stream of N_2 (15 mL min^{-1}) for 30 min to remove air and water while the temperature of the reactor was raised to 170 °C at a ramp rate of 5 °C min^{-1}. Then HCl (13.2 mL min^{-1}) was injected and the catalyst was activated at 170 °C for 30 min. Finally, a mixture of HCl (13.2 mL min^{-1}) and C_2H_2 (12 mL min^{-1}) was introduced into the reactor for the catalytic reaction, and the C_2H_2 gas hourly space velocity (GHSV(C_2H_2)) was controlled at 360 h^{-1} throughout the catalytic reaction, and the volumes of catalyst were 1 mL and 4 mL for GHSV(C_2H_2) of 720 h^{-1} and 90 h^{-1}, respectively, and other test conditions were unchanged. The gaseous product of the reaction was purified and sent to a Gas Chromatograph (Shimadzu GC-2014C) for analysis to calculate the conversion of acetylene (X_A) and selectivity to VCM (S_{VCM}):

$$X_A = \frac{\Phi_{A0} - \Phi_A}{\Phi_{A0}} \times 100\% \#(3)$$

$$S_{VCM} = \frac{\Phi_{VC}}{1 - \Phi_A} \times 100\% \#(4)$$

The calculation of The VCM space-time yield (STY, g mL^{-1} h^{-1}) of the catalyst is calculated according to (3).

$$STY = \frac{V_{C_2H_2} * 60 * X_A * S_{VCM} * 62.5}{1000 * 22.4 * V_{cat}} \# (5)$$

where Φ_{A0} is defined as the volume fraction of acetylene in the feedstock gas, Φ_A is defined as the volume fraction of remaining acetylene in the product gas, and Φ_{VC} is the volume fraction of VCM in the product gas. $V_{C_2H_2}$ is the volume flow of acetylene and *V*cat is the volume of catalyst.

2. Supplementary Figures

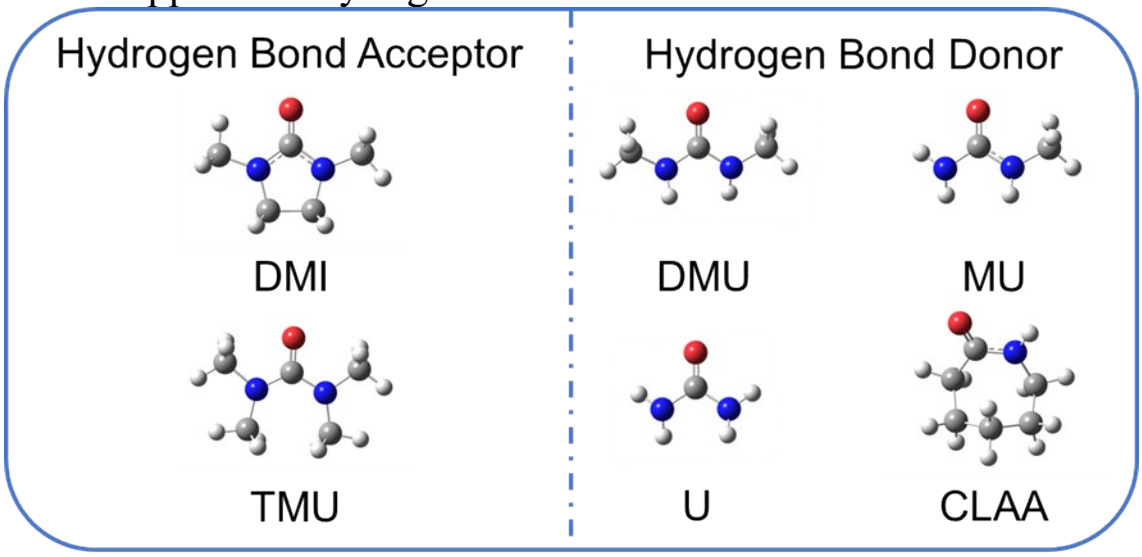

Fig. S1 Chemical structure and abbreviation of HBAs and HBDs used.

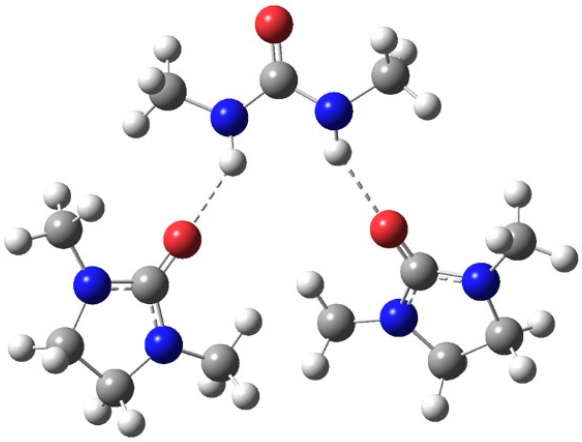

Fig. S2 Hydrogen bond structure of 2DMI-DMU.

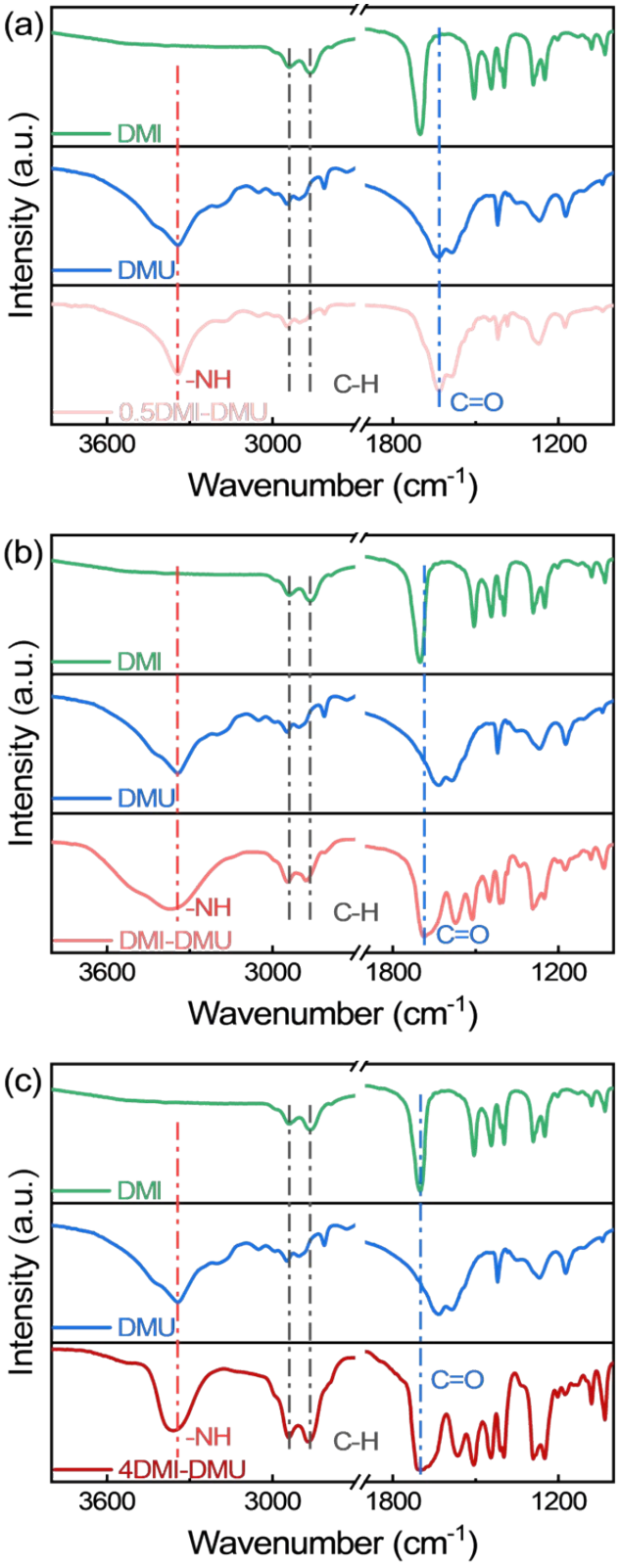

Fig. S3 FT-IR spectrum of (a) 0.5DMI-DMU, (b) 1DMI-DMU and (c) 4DMI-DMU.

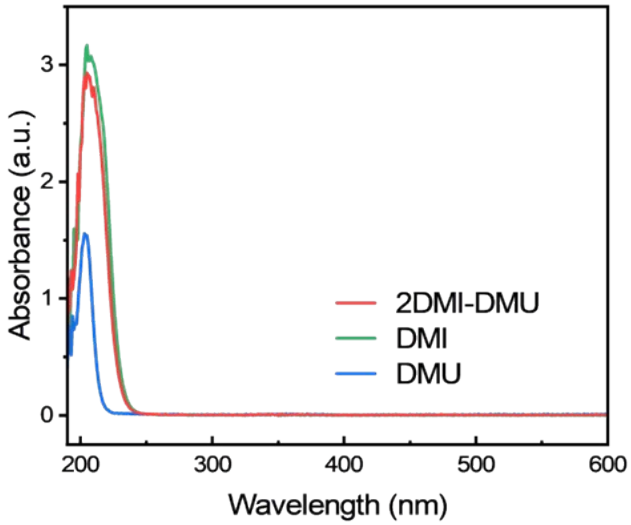

Fig. S4 UV-Vis spectra of 2DMI-DMU, DMI and DMU.

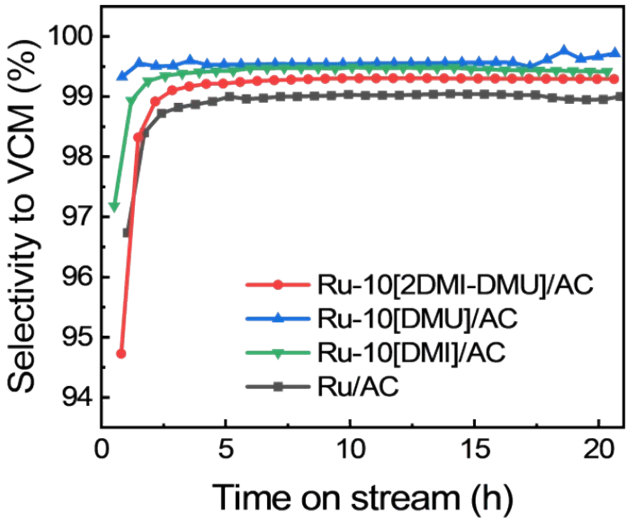

Fig. S5 Selectivity to VCM (a) for Ru-10[2DMI-DMU]/AC, Ru-10[DMU]/AC, Ru-10[DMI]/AC and Ru/AC catalysts. Reaction conditions: T = 170 °C, GHSV(C_2H_2) = 360 h^{-1}, and $V_{HCl}/V_{C_2H_2}$ = 1.1.

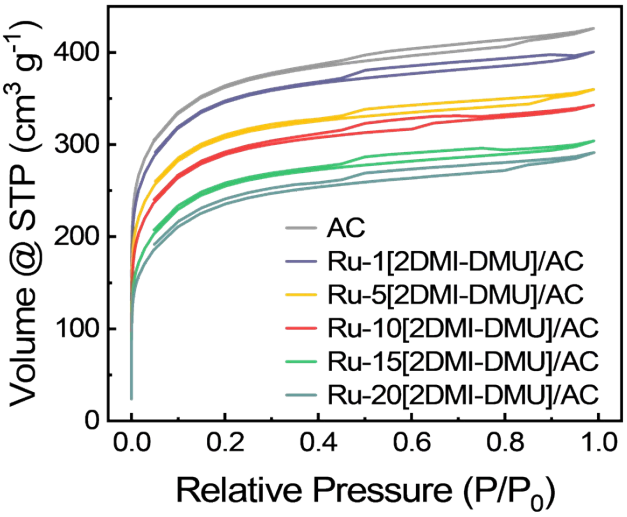

Fig. S6 He adsorption-desorption isotherms of Ru-x[2DMI-DMU]/AC catalysts.

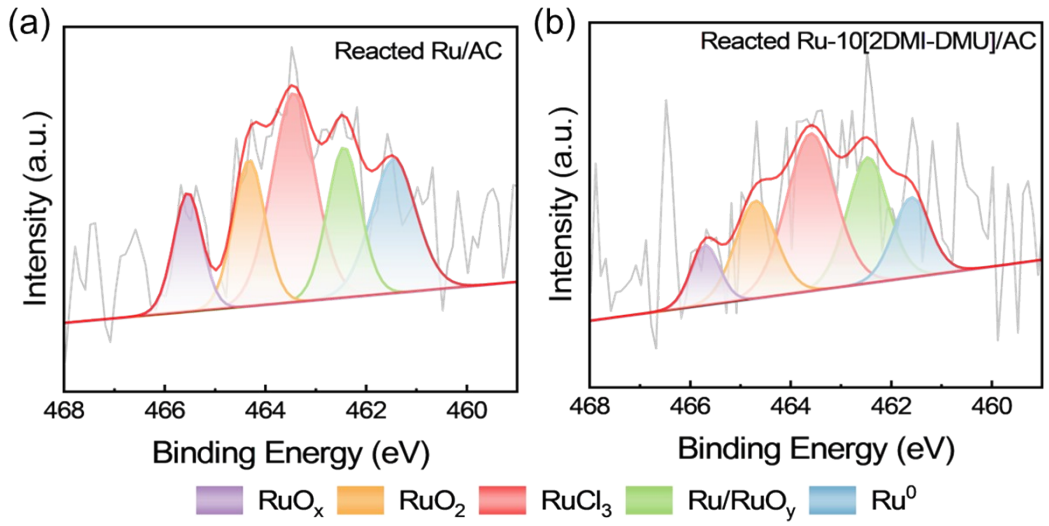

Fig. S7 Ru3p XPS spectra of the reacted Ru-based catalysts.

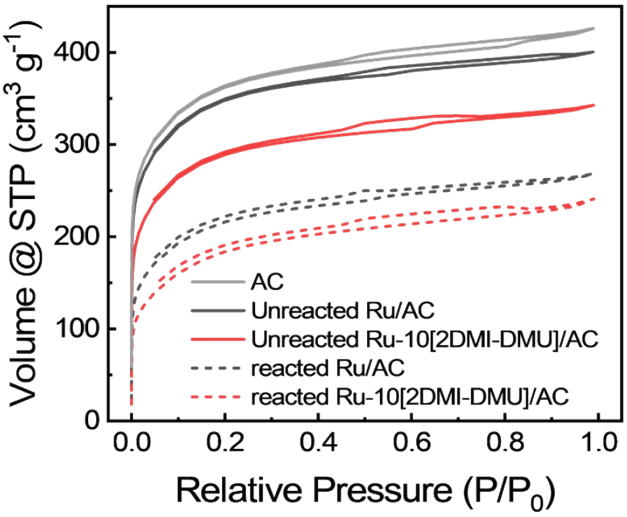

Fig. S8 He adsorption-desorption isotherms of the unreacted and reacted Ru-based catalysts.

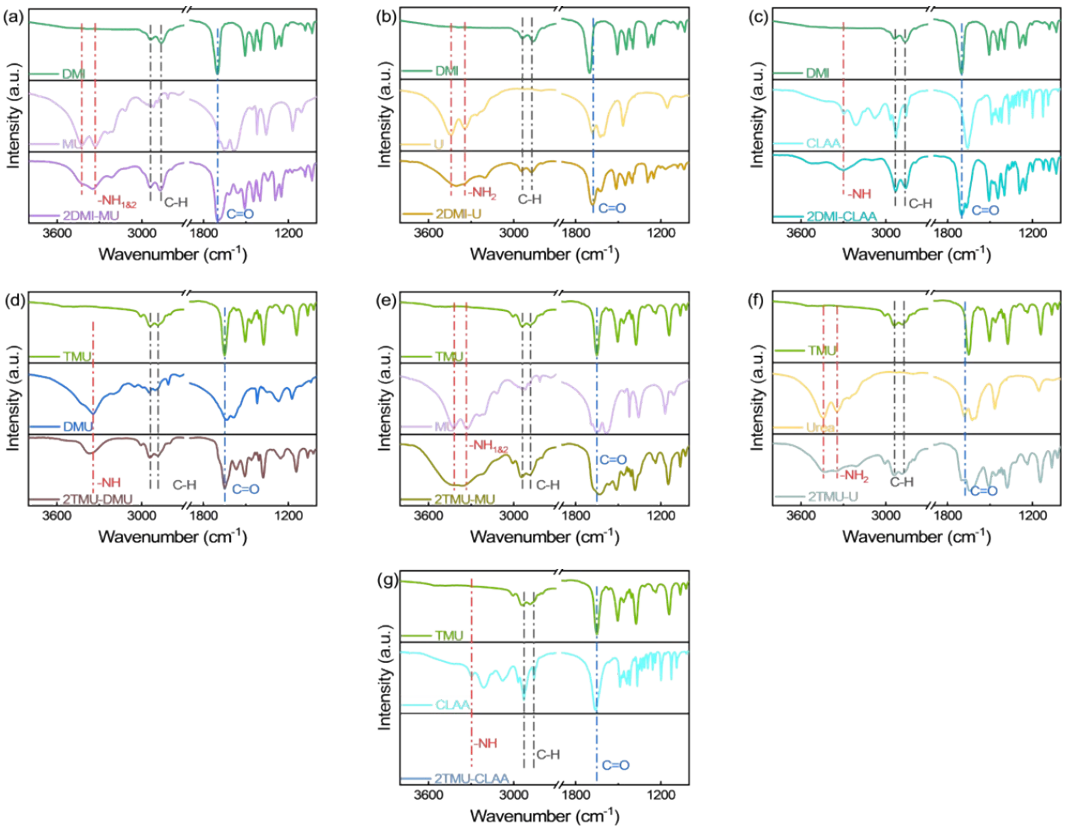

Fig. S9 FT-IR spectrum of (a) 2DMI-MU, (b) 2DMI-Urea, (c) 2DMI-CLAA, (d) 2TMU-DMU, (e) 2TMU-MU, (f) 2TMU-U and (g) 2TMU-CLAA.

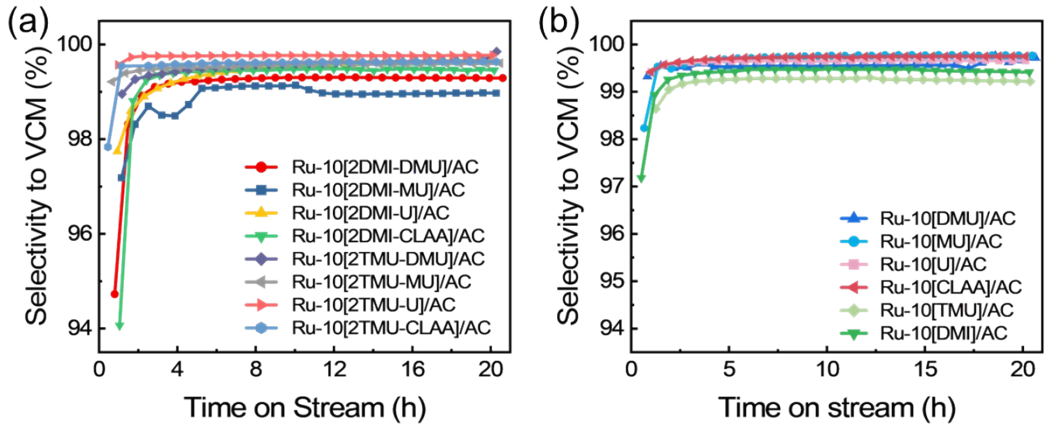

Fig. S10 Selectivity to VCM for (a) Ru-10[DES]/AC and (b) Ru-10[HBD]/AC and Ru-10[HBA]/AC catalysts. Reaction conditions: T = 170 °C, GHSV(C_2H_2) = 360 h^{-1}, and $V_{HCl}/V_{C_2H_2}$ = 1.1.

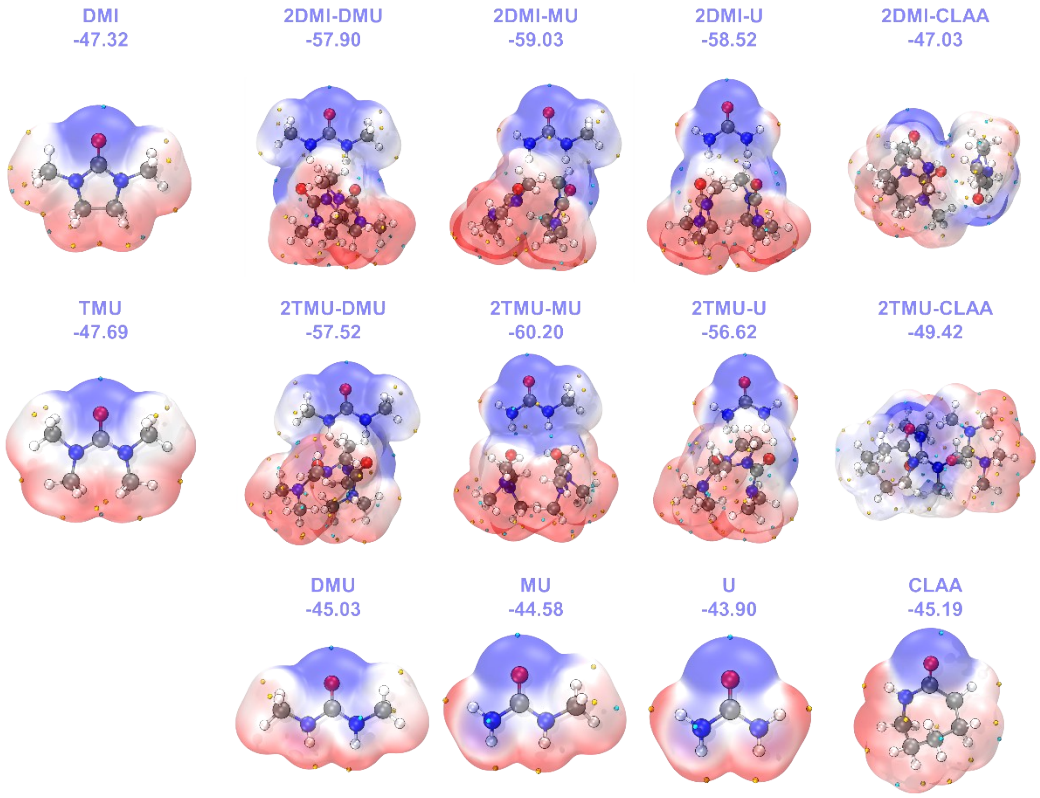

Fig. S11 ESP (kcal mol^{-1}) on the vdW surfaces of HBD, HBA and DES.

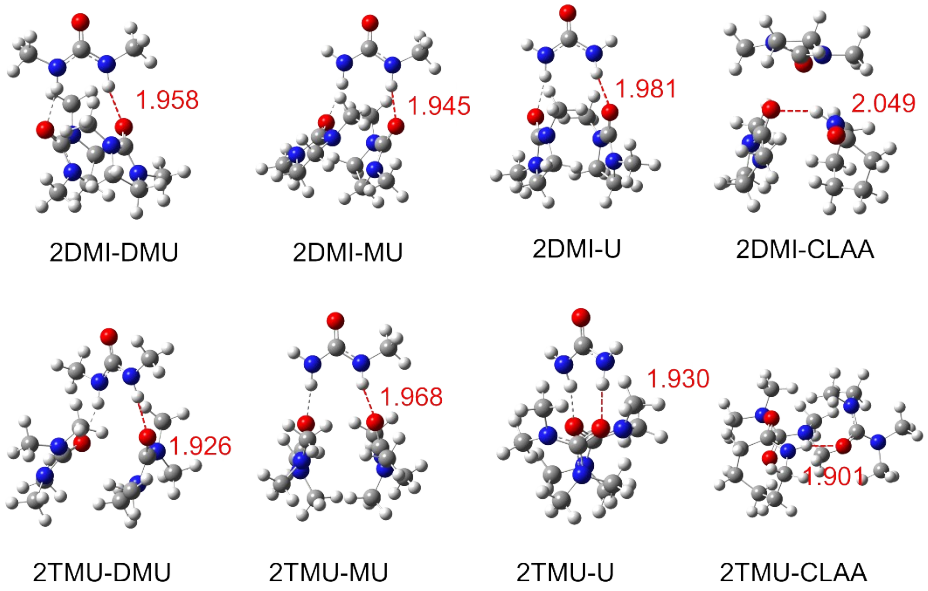

Fig. S12 Hydrogen bond length (HBL, Å) of DES.

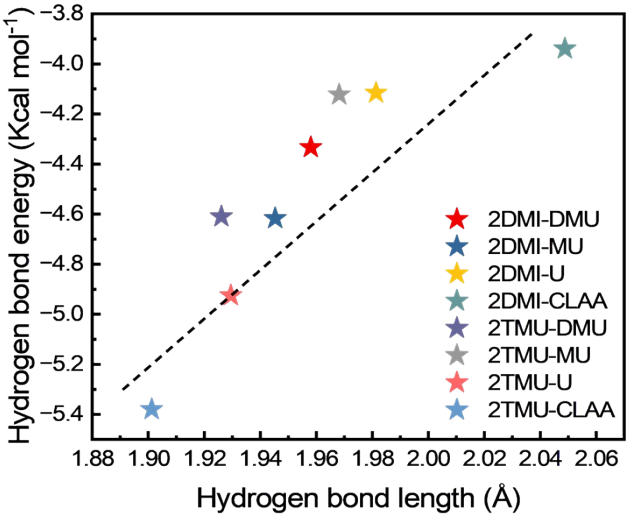

Fig. S13 Relationship between HBL and E_{HB} for DES.

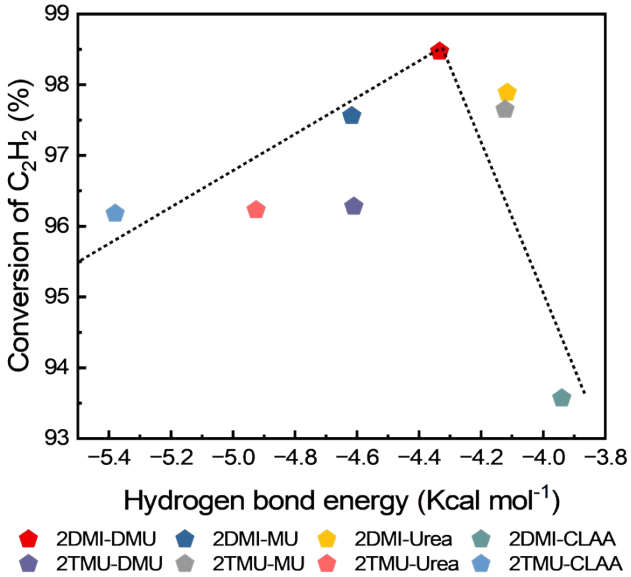

Fig. S14 Correlation of E_{HB} of DESs with Conversion of C_2H_2 over Ru-10[DES]/AC catalysts

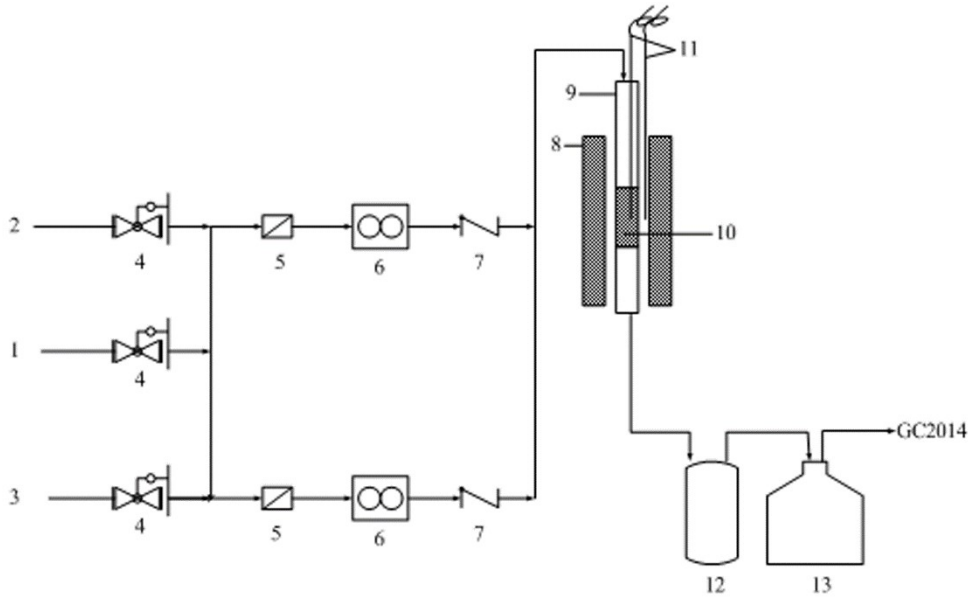

Fig. S15 Catalyst experimental setup. 1. nitrogen, 2. hydrogen chloride, 3. acetylene, 4. pressure relief valve, 5. filter, 6. mass flowmeter, 7. one-way check valve, 8. heating furnace, 9. reactor, 10. catalyst, 11. thermocouple, 12. buffer tank, 13. absorption bottle.

3. Supplementary Tables

Table S1 Pore structure parameters of Ru-x[2DMI-DMU]/AC catalysts

Catalyst	S_{BET}[a] ($m^2\ g^{-1}$)	$S_{micro.}$[b] ($m^2\ g^{-1}$)	$S_{ext.}$[c] ($m^2\ g^{-1}$)	V_P[d] ($cm^3\ g^{-1}$)	$V_{micro.}$[e] ($cm^3\ g^{-1}$)	D_{pore}[f] (nm)
AC	1326	1122	204	0.659	0.477	1.988
Ru-1[2DMI-DMU]/AC	1264	1079	185	0.620	0.459	1.960
Ru-5[2DMI-DMU]/AC	1125	962	163	0.557	0.409	1.979
Ru-10[2DMI-DMU]/AC	1053	887	167	0.530	0.379	2.013
Ru-15[2DMI-DMU]/AC	926	766	160	0.470	0.329	2.032
Ru-20[2DMI-DMU]/AC	852	685	167	0.451	0.296	2.115

[a] S_{BET}: BET specific surface area; [b] t-plot micropore area; [c] t-plot external surface area; [d] V_P: total pore volume, volume at $p/p_0 = 0.98$; [e] t-plot micropore volume; [f] Adsorption average pore width (4V/A by BET).

Table S2 The catalytic performance of the Ru-based catalysts for acetylene hydrochlorination recently reported in the literature

Catalysts	Ligands/ionic liquids	Ru content (wt%)	Reaction temperature (℃)	GHSV(C_2H_2) (h^{-1})	$V_{HCl}/V_{C_2H_2}$	Initial maximum C_2H_2 conversion (%)	STY (g mL^{-1} h^{-1})[a]	Ref.
Ru-10%Foli/AC	Formamide	1	150	360	1.15	93.9	0.934	[11]
IPr–(Ru)/AC	N-heterocyclic carbene	1	180	180	1.15	99	0.492	[12]
Ru-Thi/AC	thiourea	1	170	400	1.1	85.1	0.940	[13]
Ru-L_8/AC	1-Isopropylimidazole	1	180	720	1.15	85	1.691	[14]
Ru15%TBAH/AC	Tetrabutylammonium hexafluorophosphate	1	170	360	1.1	99	0.984	[15]
1Ru-5IL_5/AC	Butyl(triphenyl)phosphonium chloride	1	180	720	1.15	93.9	1.868	[16]
1%Ru@15%TPPB/AC	Tetraphenylphosphonium bromide	1	170	360	1.15	99.7	0.991	[17]
Ru10%[BMIM]BF_4/AC	1-Butyl-3-methylimidazolium tetrafluoroborate	1	170	360	1.1	99.0	0.984	[18]
Ru-10[2DMI-DMU]/AC	2DMI-DMU	1	170	360	1.1	98.7	0.981	This work
Ru-10[2DMI-DMU]/AC	2DMI-DMU	1	170	720	1.1	93.1	1.852	This work

[a]: The S_{VCM} of all catalysts is about 99%.

Table S3 Mulliken charge changes of O, Ru and Cl in the Ru complexes

Catalyst	The Mulliken charges of atoms (eV)					
	O	Ru	Cl_1	Cl_2	Cl_3	Sum ($RuCl_3$)
$RuCl_3$		1.144	-0.426	-0.359	-0.359	0
DMI	-0.420					
Ru-[DMI]	-0.338	0.891	-0.641	-0.329	-0.297	-0.376
DMU	-0.400					
Ru-[DMU]	-0.285	1.034	-0.584	-0.546	-0.297	-0.393
2DMI-DMU	-0.415					
Ru-[2DMI-DMU]	-0.306	0.829	-0.653	-0.352	-0.326	-0.502

Table S4 The binding energy and relative content of Ru species in the Ru-based catalysts

Catalyst	(Binding energy (eV)), area (%)										
	Ru^0		Ru/RuO_y		$RuCl_3$		RuO_2		RuO_x		$Ru^{m+}(m>0)$
Unreacted Ru/AC	(461.6)	12.3	(462.2)	10.4	(463.3)	35.3	(464.4)	26.1	(465.7)	15.8	87.7
Unreacted Ru-10[DMI]/AC	(461.6)	12.2	(462.3)	20.2	(463.3)	39.7	(464.5)	16.8	(465.5)	11.2	87.8
Unreacted Ru-10[DMU]/AC	(461.7)	11.4	(462.5)	25.8	(463.4)	34.2	(464.7)	20.1	(465.8)	8.5	88.6
Unreacted Ru-10[2DMI-DMU]/AC	(461.6)	10.2	(462.7)	29.5	(463.9)	32.0	(464.9)	15.4	(466.4)	13.0	89.8
Reacted Ru/AC	(461.5)	17.4	(462.4)	19.4	(463.4)	36.1	(464.3)	16.0	(465.5)	11.0	82.6
Reacted Ru-10[2DMI-DMU]/AC	(461.6)	13.6	(462.5)	24.4	(463.6)	37.2	(464.7)	16.0	(465.7)	8.9	86.4

Table S5 Adsorption energies of C_2H_2, HCl and VCM on the Ru complexes

	E_{ad} (kcal mol^{-1})		
	C_2H_2	HCl	VCM
DMI	-8.4	-13.4	—
DMU	-5.4	-10.5	—
2DMI-DMU	-6.7	-15.2	—
$RuCl_3$	-32.1	-16.7	-40.3
Ru-DMI	-19.1	-10.5	-22.2
Ru-DMU	-23.2	-11.5	-25.4
Ru-[2DMI-DMU]	-18.8	-9.03	-21.2

Table S6 Pore structure parameters of Ru-based catalysts

Catalyst	S_{BET}[a] ($m^2\ g^{-1}$)	ΔS_{BET}	$S_{micro.}$[b] ($m^2\ g^{-1}$)	$\Delta S_{micro.}$	$S_{ext.}$[c] ($m^2\ g^{-1}$)	V_P[d] ($cm^3\ g^{-1}$)	ΔV_P	$V_{micro.}$[e] ($cm^3\ g^{-1}$)	$\Delta V_{micro.}$
Unreacted Ru/AC	1269	489	1086	467	183	0.619	0.205	0.464	0.196
Reacted Ru/AC	780		619		161	0.415		0.268	
Unreacted Ru-10[2DMI-DMU]/AC	1053	395	887	408	167	0.530	0.157	0.379	0.169
Reacted Ru-10[2DMI-DMU]/AC	658		479		179	0.373		0.210	

[a] S_{BET}: BET specific surface area; [b] t-plot micropore area; [c] t-plot external surface area; [d] V_P: total pore volume, volume at $p/p_0 = 0.98$; [e] t-plot micropore volume; [f] Adsorption average pore width (4V/A by BET).

Table S7 Mulliken charge changes of Ru and Cl in the Ru complexes

	The Mulliken charges of atoms (eV)				
	Ru	Cl_1	Cl_2	Cl_3	Sum
$RuCl_3$	1.144	-0.426	-0.359	-0.359	0
Ru-[DMU]	1.034	-0.584	-0.546	-0.297	-0.393
Ru-[2DMI-DMU]	0.829	-0.653	-0.352	-0.326	-0.502
Ru-[2TMU-DMU]	1.053	-0.705	-0.494	-0.263	-0.409
Ru-[MU]	0.902	-0.595	-0.313	-0.302	-0.308
Ru-[2DMI-MU]	0.781	-0.747	-0.259	-0.155	-0.380
Ru-[2TMU-MU]	0.789	-0.721	-0.144	-0.326	-0.402
Ru-[U]	0.912	-0.596	-0.304	-0.303	-0.291
Ru-[2DMI-U]	1.013	-0.652	-0.480	-0.294	-0.413
Ru-[2TMU-U]	1.064	-0.641	-0.524	-0.307	-0.408
Ru-[CLAA]	0.99	-0.69	-0.257	-0.252	-0.209
Ru-[2DMI-CLAA]	1.054	-0.721	-0.419	-0.310	-0.396
Ru-[2TMU-CLAA]	0.792	-0.711	-0.338	-0.214	-0.471

Table S8 The HBL and E_{HB} of DES

DES	HBL (Å)	E_{HB} (Kcal mol^{-1})
2DMI-DMU	1.958	-4.334
2DMI-MU	1.945	-4.617
2DMI-Urea	1.981	-4.116
2DMI-CLAA	2.049	-3.940
2TMU-DMU	1.926	-4.610
2TMU-MU	1.968	-4.123
2TMU-Urea	1.930	-4.925
2TMU-CLAA	1.901	-5.380

4. References

1 S. Grimme, J. Antony, S. Ehrlich and H. Krieg, *J Chem Phys*, 2010, **132**, 154104.

2 M. J. Frisch, G. W. Trucks, H. B. Schlegel, G. E. Scuseria, M. A. Robb, J. R. Cheeseman, G. Scalmani, V. Barone, G. A. Petersson, H. Nakatsuji, X. Li, M. Caricato, A. V. Marenich, J. Bloino, B. G. Janesko, R. Gomperts, B. Mennucci, H. P. Hratchian, J. V. Ortiz, A. F. Izmaylov, J. L. Sonnenberg, D. Williams-Young, F. Ding, F. Lipparini, F. Egidi, J. Goings, B. Peng, A. Petrone, T. Henderson, D. Ranasinghe, V. G. Zakrzewski, J. Gao, N. Rega, G. Zheng, W. Liang, M. Hada, M. Ehara, K. Toyota, R. Fukuda, J. Hasegawa, M. Ishida, T. Nakajima, Y. Honda, O. Kitao, H. Nakai, T. Vreven, K. Throssell, J. A. Montgomery Jr., J. E. Peralta, F. Ogliaro, M. J. Bearpark, J. J. Heyd, E. N. Brothers, K. N. Kudin, V. N. Staroverov, T. A. Keith, R. Kobayashi, J. Normand, K. Raghavachari, A. P. Rendell, J. C. Burant, S. S. Iyengar, J. Tomasi, M. Cossi, J. M. Millam, M. Klene, C. Adamo, R. Cammi, J. W. Ochterski, R. L. Martin, K. Morokuma, O. Farkas, J. B. Foresman and D. J. Fox, *Journal*, 2016.

3 K. Eichkorn, F. Weigend, O. Treutler and R. Ahlrichs, *Theoretical Chemistry Accounts*, 1997, **97**, 119-124.

4 B. Miehlich, A. Savin, H. Stoll and H. Preuss, *Chem. Phys. Lett.*, 1989, **157**, 200-206.

5 Y. Zhao and D. G. Truhlar, *The Journal of Physical Chemistry A*, 2008, **112**, 6794-6799.

6 Y. Zhao and D. G. Truhlar, *The Journal of Chemical Physics*, 2006, **125**, 194101.

7 F. Weigend and R. Ahlrichs, *Phys. Chem. Chem. Phys.*, 2005, **7**, 3297-3305.

8 T. Lu and F. Chen, *J. Comput. Chem.*, 2012, **33**, 580-592.

9 T. Lu and F. Chen, *J. Mol. Graph. Model.*, 2012, **38**, 314-323.

10 S. Emamian, T. Lu, H. Kruse and H. Emamian, *J. Comput. Chem.*, 2019, **40**, 2868-2881.

11 Y. Li, F. Wang, J. Hu, M. Sun, J. Wang and X. Zhang, *Catal. Sci. Technol.*, 2021, **11**, 7347-7358.

12 M. Cai, H. Zhang, B. Man, J. Li, L. Li, Y. Li, D. Xie, R. Deng and J. Zhang, *Catal. Sci. Technol.*, 2020, **10**, 3552-3560.

13 X. Wang, G. Lan, Z. Cheng, W. Han, H. Tang, H. Liu and Y. Li, *Chin. J. Catal.*, 2020, **41**, 1683-1691.

14 J. Li, H. Zhang, M. Cai, L. Li, Y. Li, R. Zhao and J. Zhang, *Appl. Catal., A*, 2020, **592**, 117431.

15 H. You, H. Zhang, L. Yu, N. Yao, L. Wei and J. Zhang, *Catal. Today*, 2020, **355**, 205-213.

16 J. Li, H. Zhang, L. Li, M. Cai, Y. Li, D. Xie and J. Zhang, *ACS Sustainable Chem. Eng.*, 2020, **8**, 10173-10184.

17 S. Shang, W. Zhao, Y. Wang, X. Li, J. Zhang, Y. Han and W. Li, *ACS Catal.*, 2017, **7**, 3510-3520.

18 Y. Li, Y. Dong, W. Li, Y. Han and J. Zhang, *Mol. Catal.*, 2017, **443**, 220-227.